Cell Reports, Volume *39*

Supplemental information

Dimerization-dependent membrane tethering by Atg23 is essential for yeast autophagy

Wayne D. Hawkins, Kelsie A. Leary, Devika Andhare, Hana Popelka, Daniel J. Klionsky, and Michael J. Ragusa

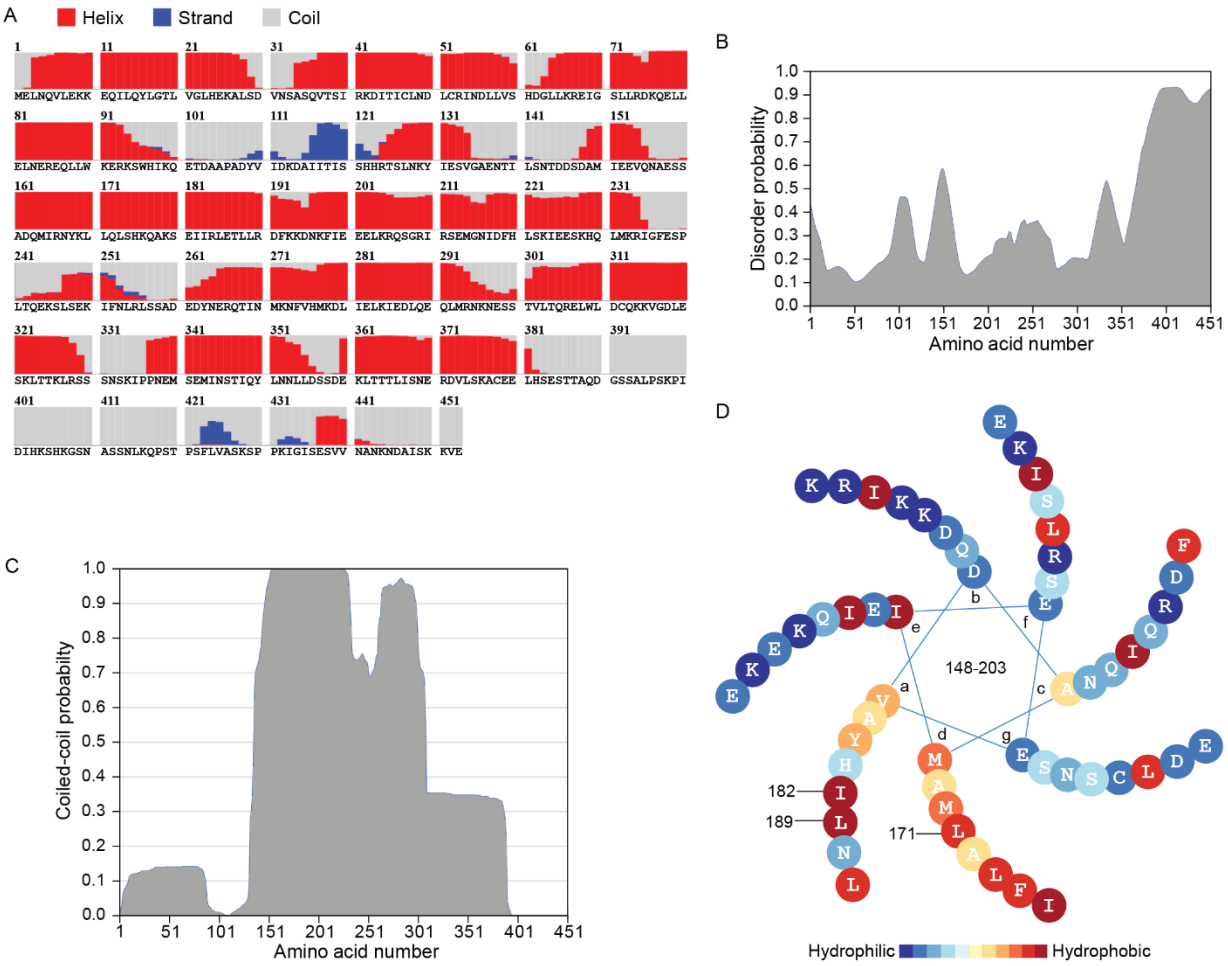

Figure S1. Atg23 is primarily α-helical with a disordered C terminus and at least one coiled-coil domain. Related to Figures 1 and 2. (A) Secondary structure prediction of Atg23 using the RaptorX Property server. (B) Disorder probability prediction of Atg23 as calculated with MFDp2. (C) Coiled-coil probability for Atg23 as determined using MultiCoil2. (D) Heptad repeat helical wheel of Atg23 amino acids 148-203 with hydrophobic residues shown in yellow, orange or red and hydrophilic residues shown in blue. Constituent residues of the Atg23[LIL] mutant are labeled.

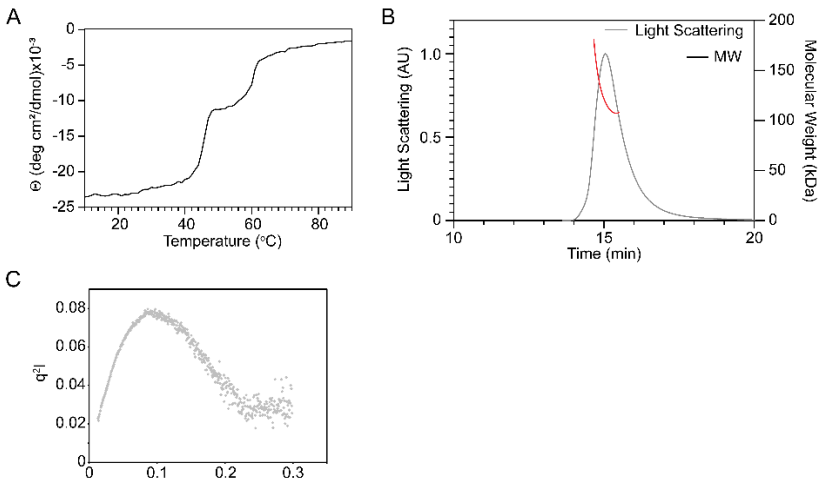

Figure S2. Additional biophysical characterization of Atg23. Related to Figure 1. (A) Temperature unfolding curve of Atg23 was monitored by circular dichroism at 222 nm. Two unfolding events were observed at 46°C and 61°C. (B) Light scattering data of Atg23 are shown as arbitrary units (AU) vs elution time in minutes. Molecular weight is shown in kDa. (C) Kratky plot of Atg23.

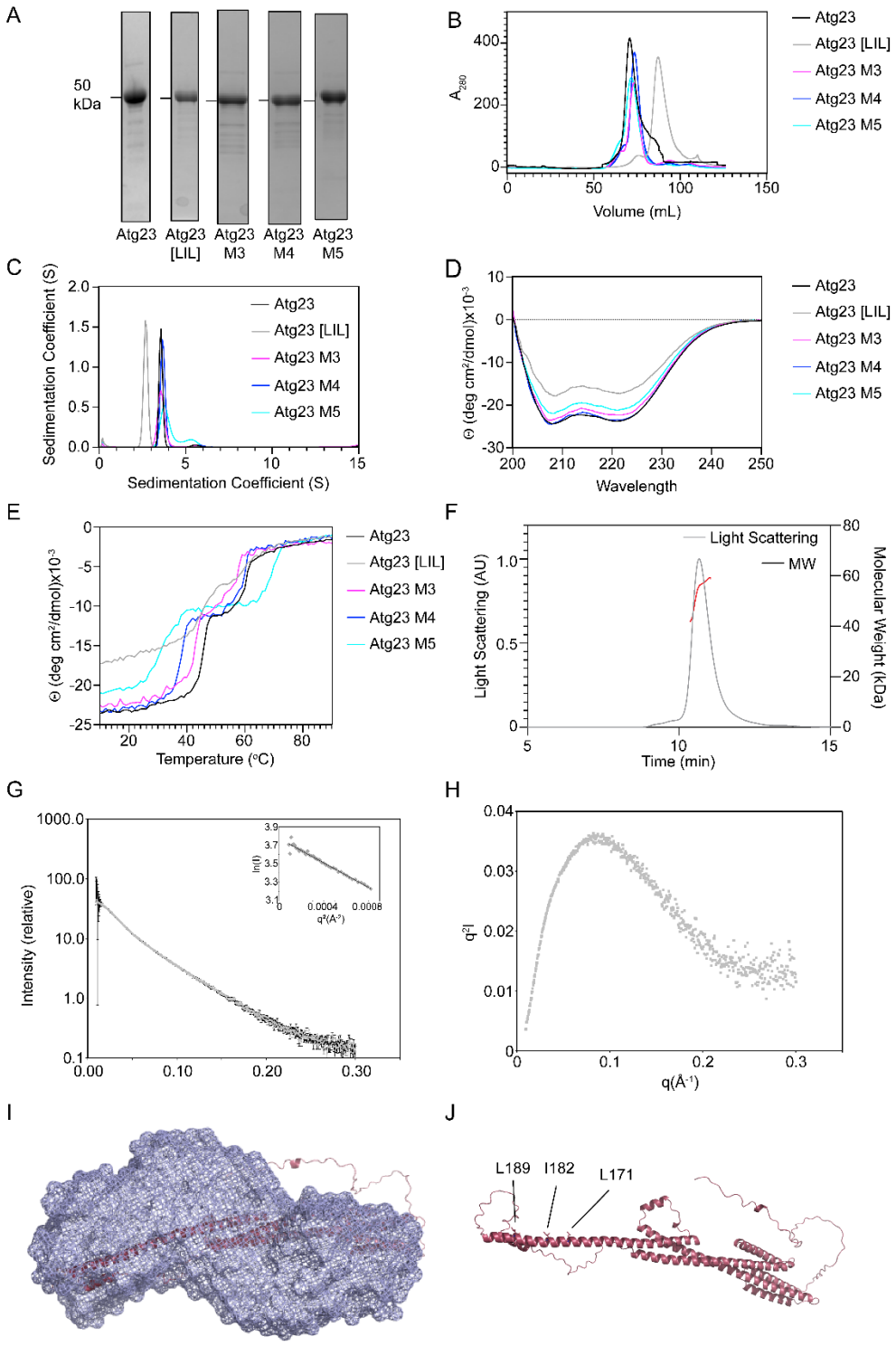

Figure S3. Protein purification and biophysical characterization of Atg23 mutants. Related to Figures 2 and 3. (A) SDS-PAGE gels of purified Atg23, Atg23[LIL], M3, M4 and M5. (B) Overlay of SEC chromatograms of Atg23, M3, M4, M5 and Atg23[LIL] with elution volumes of 61 kDa and 75 kDa, respectively. (C) Analytical ultracentrifugation of Atg23 WT, M3, M4 and M5, which are dimeric, and Atg23[LIL] which is monomeric. (D) Circular dichroism spectra of M3, M4 and M5 overlayed with Atg23 and Atg23[LIL]. All mutants retain the α-helical secondary structure.

(E) Temperature unfolding curves of Atg23 M3, M4, M5 and Atg23[LIL] were monitored by circular dichroism at 222 nm. Based on the unfolding events, M3-M5 are increasingly less thermostable. (F) Light scattering data of Atg23[LIL] is shown as arbitrary units (AU) vs elution time in minutes. Molecular weight is shown in kDa. (G) SAXS data for Atg23[LIL]. The Guinier plot is shown as an inset. (H) Kratky plot for Atg23[LIL]. (I) The Atg23 model from the AlphaFold Protein Structure Database is shown as a cartoon representation in red docked into the SAXS envelope for Atg23[LIL]. (J) The Atg23 model from the AlphaFold Protein Structure Database is shown as a cartoon representation where L171, I182 and L189 are depicted as stick representations and labeled.

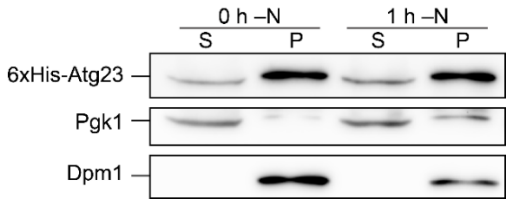

Figure S4. Subcellular fractionation of SEY6210 yeast cells expressing 6xHis-Atg23 on the pRS-424 plasmid. Related to Figure 3. Cells were subjected to nitrogen starvation for 0 or 1 h prior to harvesting. Pgk1 and Dpm1 are markers for the cytosolic and membrane fractions, respectively. P, pellet (membrane); S, supernatant (cytosol).

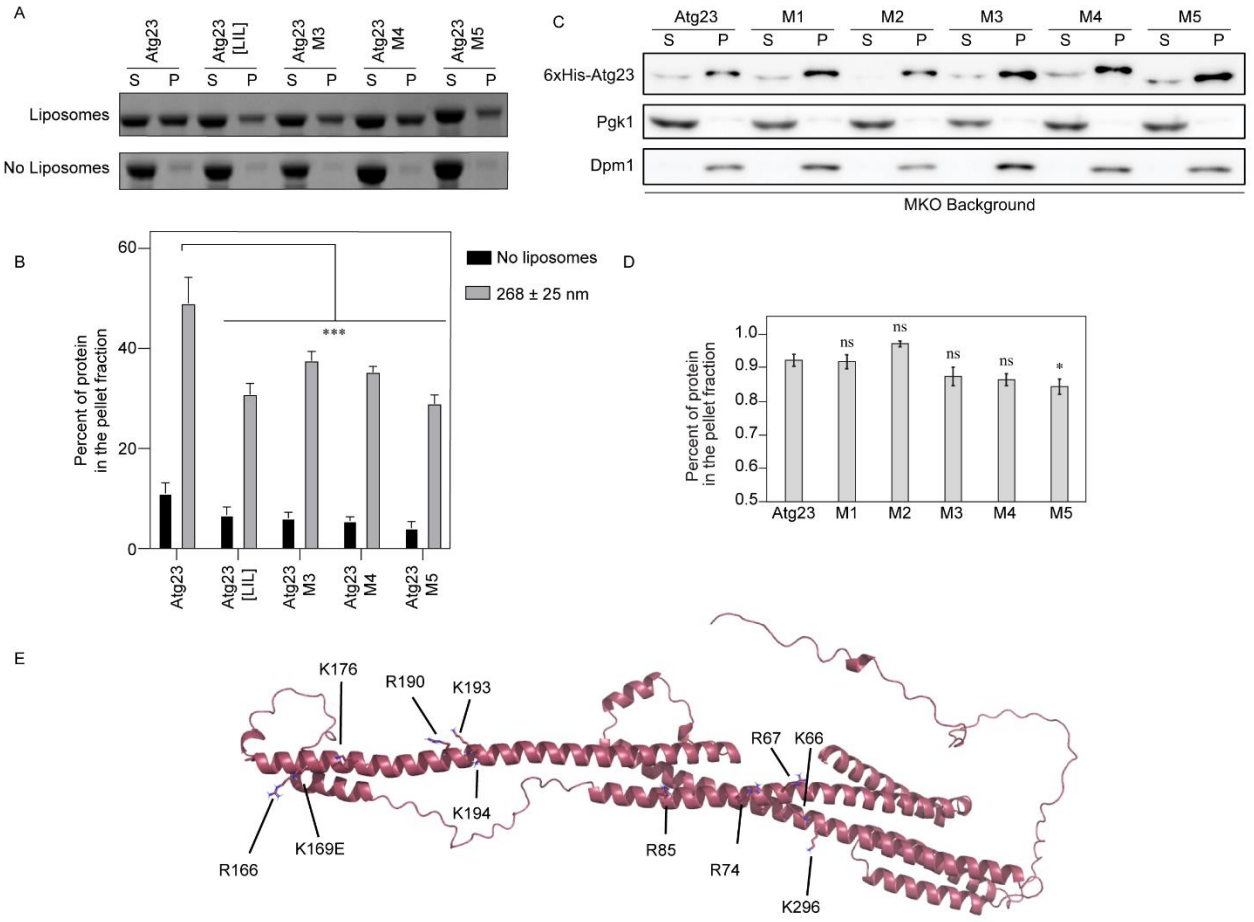

Figure S5. Mutation of positively charged residues reduces membrane binding. Related to Figure 3. (A) Liposome sedimentation assays were conducted with Atg23, Atg23[LIL], M3, M4 and M5 with YPL liposomes at 100 mM NaCl. Representative SDS-PAGE gels containing the supernatant (S) and pellet (P) fractions are shown. (B) The percent of protein in the pellet fraction in A was quantified by densitometry. Error bars represent the standard deviation from four experiments. Statistical significance was determined by two-way ANOVA with Tukey's multiple comparison test. ***, $p<0.001$; ns, not significant relative to the wildtype Atg23 with liposomes. (C) Wild-type or mutated 6xHis-Atg23 was overexpressed in the MKO background and analyzed by subcellular fractionation. (D) Quantification of subcellular fractionation results from four biological replicates. Error bars represent s.e.m., *, $p=0.03$ by two-sample t-test. (E) The Atg23 model from the AlphaFold Protein Structure Database is shown as a cartoon representation with each positively charged amino acid mutated shown as a stick representation. The five Atg23 mutants generated were R166E, K169E, K176E (M1), R190E, K193E, K194E (M2), K66E, R67E (M3), K66E, R67E, K296E (M4) and K66E, R67E, R74E, R85E, K296E (M5).

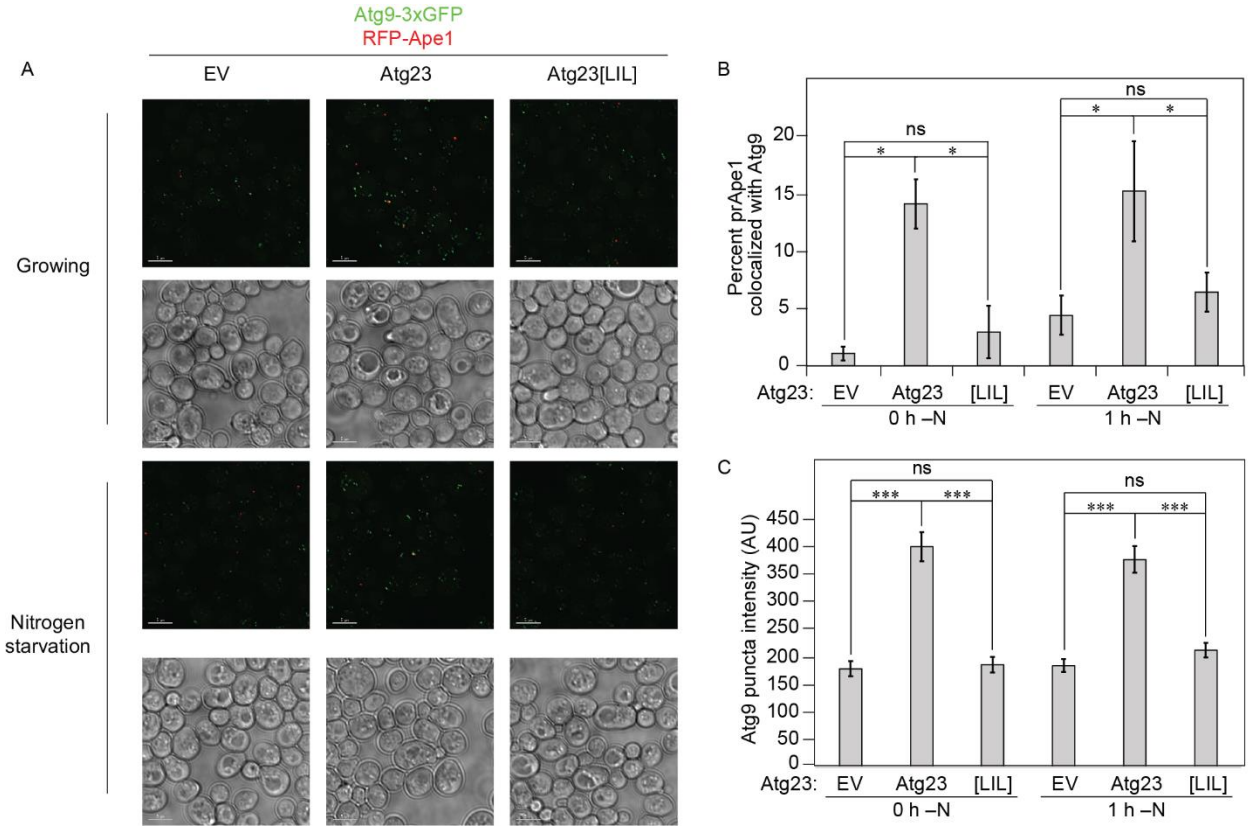

Figure S6. Atg23[LIL] is defective in Atg9 organization at the peripheral sites. Related to Figure 4. (A) Representative images of Atg9-3xGFP and RFP-Ape1 in the absence of Atg11 and presence of empty vector, Atg23 or Atg23[LIL] grown in either nutrient-rich or nitrogen-starvation medium for 1 h prior to microscopy. Scale bars: 5 μm. (B) Quantification of the average number of puncta per cell. Error bars represent s.e.m. n>10 images; *, $p<0.05$ by two-sample t-test. (C) Quantification of the Atg9 puncta intensity. Error bars represent s.e.m. n=150 puncta; ***, $p<0.001$ by two-sample t-test.

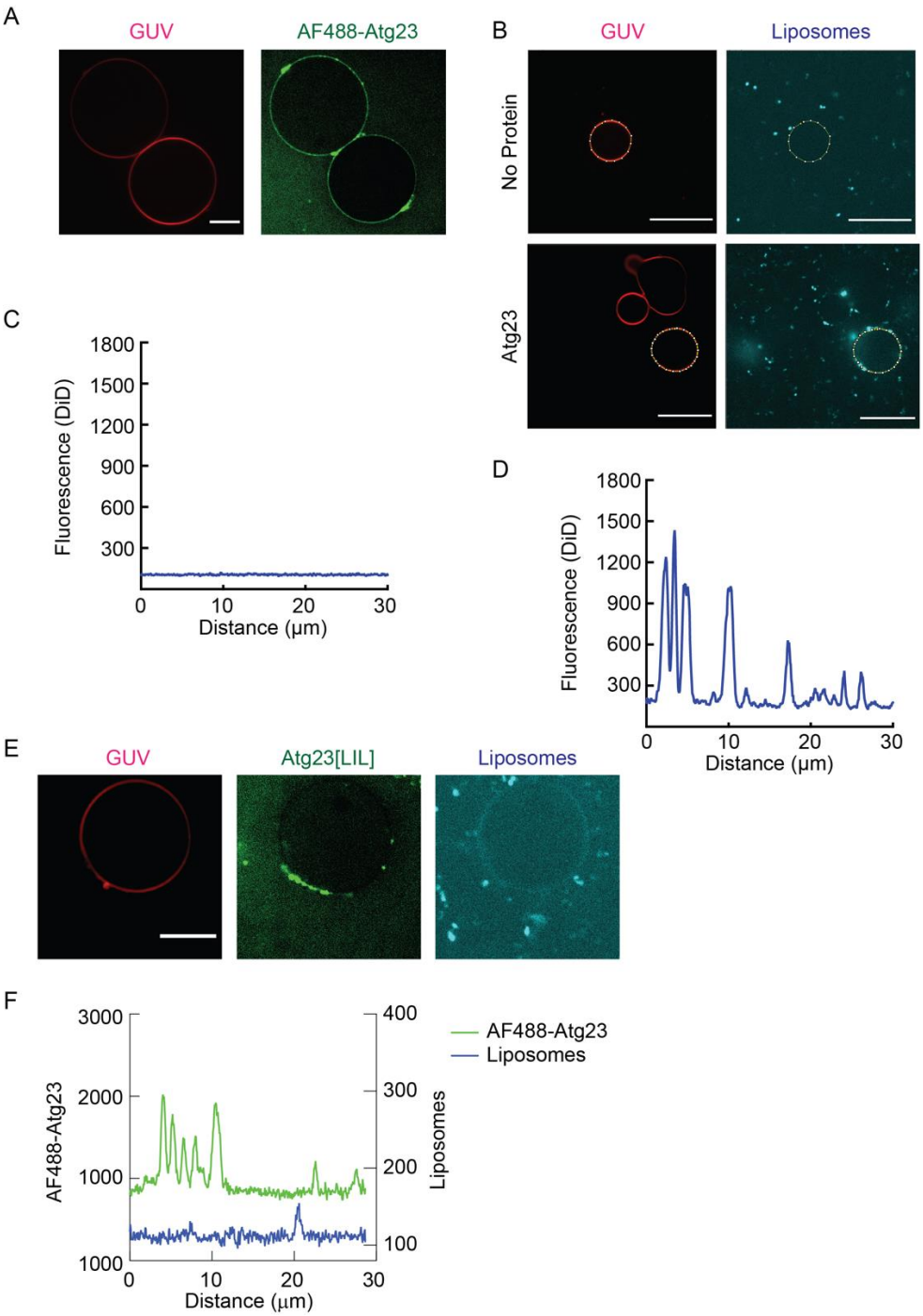

Figure S7. Atg23 binding to GUVs and intensity profiles of GUVs showing liposome tethering. Related to Figure 5. (A) Representative images showing Alexa Fluor$_{488}$ (AF488)-Atg23 (green) bound to YPL GUVs (red). (B) Representative images of GUVs in the absence (top panels) and presence of Atg23 (bottom panels). DiD intensity was plotted using a segmented line placed along the GUVs (dashed yellow line). (C) Quantification of the no-protein control shows uniform low intensity for the DiD Fluorescence along the GUVs. (D) Quantification of the DiD intensity along the GUVs in the presence of Atg23 shows sharp peaks corresponding to tethered liposomes. Scale bar: 10 μm in A and 20 μm in B. (E) Representative image showing AF488-ATG23[LIL] bound GUVs (green) incubated with liposomes (cyan). Scale bar: 10 μm. (F) Intensity profile showing

AF488-Atg23[LIL] and liposome fluorescence on a segmented line placed along the surface of the GUV in (A).

Table S1. Oligonucleotide information, related to STAR Methods.

oWH195 GCTTGATATCGAATTCCTGCAGC	IDT (this study)	N/A
oWH196 TCGATACCGTCGACCTCGAG	IDT (this study)	N/A
oWH197 CCTCGAGGTCGACGGTATCGATGCTTTTACTACTTTC GGAGTTATTAATTGCAC	IDT (this study)	N/A
oWH198 CCGGGCTGCAGGAATTCGATATCAAGCTTACTTGTA CAGCTCGTCCATGCC	IDT (this study)	N/A
oWH199 GGGGAAACAGAGAACAGTACTATAGAAGAT	IDT (this study)	N/A
oWH200 AACATTTAAACATCAAAATAAAACCCATCCAGGTAT A	IDT (this study)	N/A
oWH201 TATTGACGTCTTGTCTTCTACAATTTCTCATCC	IDT (this study)	N/A
oWH202 TAACCAATAATAATAATTTATTAACCTCTTTTTTTCTT ATTAGGCTTCTC	IDT (this study)	N/A
oWH341 CTATTGGAAGAAGAAATTGGGTCCTTACTTGAAGAC AAACAAGAG	IDT (this study)	N/A
oWH342 CCAATTTCTTCTTCCAATAGACCATCATGGGATACTA AGAGATCATT	IDT (this study)	N/A
oWH343 GAGAATTACGAACTGTTACAATTATCTCATGAGCAA GCTAAATCAGAAATAATAAGGCTGGAAACTTTATT	IDT (this study)	N/A
oWH344 CTCATGAGATAATTGTAACAGTTCGTAATTCTCTATC ATTTGATCCGCAGAAGATTCAGC	IDT (this study)	N/A
oWH345 TAGAAGACTTCGAAGAGGACAATAAATTCATTGAAG AGGAGTTAAAAAGGCAATC	IDT (this study)	N/A
oWH346 GTCCTCTTCGAAGTCTTCTAATAAAGTTTCCAGCCTT ATTATTTCTGATTTAGCTT	IDT (this study)	N/A
oWH347 ACAAGAGCTACTAGAACTGAACGAAGAAGAGCAGC TTCTTTGGAAAGAG	IDT (this study)	N/A
oWH348 TCAGTTCTAGTAGCTCTTGTTTGTCTTCAAGTAAGGA CCCAATTTCTTCTTCCAATA	IDT (this study)	N/A
oWH349 TGAGAAATGAAAATGAGTCTTCTACAGTACTAACGC AACGTGAATTATGG	IDT (this study)	N/A
oWH350 AGACTCATTTTCATTTCTCATTAGTTGCTCTTGTAGAT CTTCAATTTTCAGT	IDT (this study)	N/A
oWH351 CTATTGGAAGAAGAAATTGGGTCCTTACTTCGAGAC AAACAAGAG	IDT (this study)	N/A

oWH352 AAGTACTTCTTTTATTTTCTTTTATACATCCGTACGCTGCAGGTCGAC	IDT (this study)	N/A
oWH353 TTGTCATTTGTGACAAACGTTTAGCACTGTAATCGATGAATTCGAGCTCG	IDT (this study)	N/A
oWH354 GTGTACTGTTGTTGTTCGGAAAGTACTTCTTTTATTTTCTTTTATACATCCGTACGCTGCAGGTCGAC	IDT (this study)	N/A
oWH355 ATAGATACATAATTAAAATCTTGTCATTTGTGACAAACGTTTAGCACTGTAATCGATGAATTCGAGCTCG	IDT (this study)	N/A
oWH356 TTCTCAAATCAGAACCAAAGTAGTCCTCCTTTGAACAACGCGTACGCTGCAGGTCGAC	IDT (this study)	N/A
oWH357 TATATCCAGGAAACTTGGTAGTCGATAACAAGACTTATCGAATCGATGAATTCGAGCTCG	IDT (this study)	N/A
KAL20_Sc23_LIL_FW agaagcaataaggctggaaactttagcaAGAGACTTCAAAAAGGAC	IDT (this study)	N/A
KAL20_Sc23_LIL_RV gatttagcttgcttatgagataattgtgcCAGTTTGTAATTACGTATCATTTG	IDT (this study)	N/A
KAL21_SDM_2_FW TGGTCTATTGgaagaaGAAATTGGGTC	IDT (this study)	N/A
KAL21_SDM_2_RV TCATGGGATACTAAGAGATC	IDT (this study)	N/A
KAL21_SDM_3_FW AATGAGAAATgaaAATGAGTCTTCTAC	IDT (this study)	N/A
KAL21_SDM_3_RV AGTTGCTCTTGTAGATCTTC	IDT (this study)	N/A
KAL21_SDM_4_FW ctagaactgaacgaagaaGAGCAGCTTCTTTGGAAAG	IDT (this study)	N/A
KAL21_SDM_4_RV tagctcttgtttgtcttcAAGTAAGGACCCAATTTC	IDT (this study)	N/A
KAL_pHis2_3C_FW tttcagggcccaGCCATGGGATCCGGAATT	IDT (this study)	N/A
KAL_pHis2_3C_RV aagcacttctagGGTCGTTGGGATATCGTAATC	IDT (this study)	N/A